

## $^{13}\text{C}$ Direct Detection Experiments on the Paramagnetic Oxidized Monomeric Copper, Zinc Superoxide Dismutase

Wolfgang Bermel,<sup>†</sup> Ivano Bertini,<sup>\*,‡</sup> Isabella C. Felli,<sup>‡</sup> Rainer Kümmerle,<sup>§</sup> and Roberta Pierattelli<sup>‡</sup>

Contribution from Bruker BioSpin GmbH, Rheinstetten, Germany, CERM and Department of Chemistry, University of Florence, Sesto Fiorentino, Italy, and Bruker BioSpin AG, Fällanden, Switzerland

Received July 31, 2003; E-mail: bertini@cerm.unifi.it

**Abstract:** In this report, the use of  $^{13}\text{C}$  direct detection has been pursued in 2D experiments ( $^{13}\text{C}$ – $^{13}\text{C}$  COSY,  $^{13}\text{C}$ – $^{13}\text{C}$  COCAMQ,  $^{13}\text{C}$ – $^{13}\text{C}$  NOESY) to detect broad lines in nuclear magnetic resonance spectra of paramagnetic metalloproteins. The sample is a monomeric oxidized copper, zinc superoxide dismutase. Thanks to direct detection probeheads, cryogenic technology, and implementation of  $^{13}\text{C}$  band-selective homodecoupling, many broadened signals were detected. Proton signals for the same residues escaped detection in  $^1\text{H}$  and  $^1\text{H}$ – $^{15}\text{N}$  HSQC experiments because of the broadening. Only the  $^{13}\text{C}$  signals which experience large contact coupling escaped detection, i.e., the  $^{13}\text{C}$  nuclei of the metal coordinated histidines. Otherwise, nuclei as close to copper(II) as 4 Å can be detected. Paramagnetic-based restraints can in principle be used for solution structure determination of paramagnetic metalloproteins and in copper(II) proteins in particular. The present study is significant also for the study of large diamagnetic proteins for which proton relaxation makes proton-based spectroscopy not adequate.

### Introduction

Paramagnetic proteins in solution can be conveniently studied by nuclear magnetic resonance (NMR).<sup>1</sup> Solution structures have been determined for several such systems,<sup>2–5</sup> and in most cases the paramagnetic effects have been exploited to derive structural information useful to refine the structure.<sup>6,7</sup> The magnitude of the paramagnetic effects on nuclear relaxation rates depends on the nature of the metal ion and on its electronic relaxation rate. Depending on the metal–nucleus distance, the electron–nucleus coupling effects may prevent the observation of proton signals of the residues close to the metal site due to induced broadening of the NMR lines.<sup>8</sup>

This is the case for copper(II)-containing proteins, where protons close to the paramagnetic copper center are frequently characterized by relaxation rates that are too large to be studied

by the conventional NMR approach.<sup>9</sup> This effect is more dramatic in the so-called type II copper centers, where the lack of accessible low-energy excited states does not provide efficient electronic relaxation mechanisms. This is reflected in a long correlation time for the electron–nucleus interaction that causes large contributions to relaxation. Furthermore, if we exclude signals shifted by the Fermi-contact mechanism, many hyperfine broadened resonances fall under the ensemble of sharp signals due to the diamagnetic protons. These effects render signal detection, assignment, and determination of structural constraints very challenging, especially in what usually is the most interesting part of the protein close to the metal active site.

$^{13}\text{C}$  direct detection offers advantages for the study of paramagnetic proteins because the paramagnetic dipolar contributions to nuclear relaxation depend on the square of the gyromagnetic ratio of the observed nucleus; thus, going from  $^1\text{H}$  to  $^{13}\text{C}$  detection guarantees a decrease in relaxation rates of a factor of about 16 ( $\gamma_{\text{H}} = 2.67 \times 10^{-8} \text{ rad s}^{-1} \text{ T}^{-1}$ ;  $\gamma_{\text{C}} = 6.73 \times 10^{-7} \text{ rad s}^{-1} \text{ T}^{-1}$ ). Of course this also implies a reduction in sensitivity, but this limitation can be overcome with the use of high field spectrometers as well as hardware specifically designed for heteronuclear observation.

Detection and assignment of  $^{13}\text{C}$  resonances is the preliminary step to obtain  $^{13}\text{C}$ -based structural constraints. This has been shown for CopC, a Cu(II)-binding protein involved in copper homeostasis, where the type II copper ion causes such fast nuclear relaxation that no  $^1\text{H}$  resonances can be detected in a sphere of 11 Å from the metal ion.<sup>10,11</sup> The  $^{13}\text{C}$  direct detection

<sup>†</sup> Bruker BioSpin GmbH.

<sup>‡</sup> University of Florence.

<sup>§</sup> Bruker BioSpin AG.

- (1) Bertini, I.; Turano, P.; Vila, A. J. *Chem. Rev.* **1993**, *93*, 2833–2932.
- (2) Banci, L.; Bertini, I.; Eltis, L. D.; Felli, I. C.; Kastrau, D. H. W.; Luchinat, C.; Piccioli, M.; Pierattelli, R.; Smith, M. *Eur. J. Biochem.* **1994**, *225*, 715–725.
- (3) Bertini, I.; Luchinat, C.; Rosato, A. *Adv. Inorg. Chem.* **1999**, *47*, 251–282.
- (4) Bertini, I.; Rosato, A.; Turano, P. *Pure Appl. Chem.* **1999**, *71*, 1717–1725.
- (5) Banci, L.; Bertini, I.; Luchinat, C.; Turano, P. In *The Porphyrin Handbook*; Kadish, K. M., Smith, K. M., Guillard, R., Eds.; Academic Press: San Diego, CA, 2000; pp 323–350.
- (6) Bertini, I.; Luchinat, C.; Piccioli, M. *Methods Enzymol.* **2001**, *339*, 314–340.
- (7) Bertini, I.; Luchinat, C.; Parigi, G. *Concepts Magn. Reson.* **2002**, *14*, 259–286.
- (8) Bertini, I.; Luchinat, C.; Parigi, G. *Solution NMR of Paramagnetic Molecules*; Elsevier: Amsterdam, 2001.

(9) Banci, L.; Pierattelli, R.; Vila, A. J. *Adv. Protein Chem.* **2002**, *60*, 397–449.

approach allowed us to detect  $^{13}\text{C}$  resonances as close as 6 Å from the metal ion and to determine, through longitudinal relaxation rates, metal–nucleus distance constraints.<sup>11</sup>

Several applications of  $^{13}\text{C}$  direct detection to macromolecules have recently appeared in the literature.<sup>11–20</sup> Two-dimensional  $^{13}\text{C}$ – $^{13}\text{C}$  correlation experiments have been used to detect resonances in paramagnetic systems of nuclei at distances from the metal ion where the  $^1\text{H}$  resonances were broadened beyond detection<sup>11,12,15–18</sup> as well as to detect and assign side-chain correlations in an octameric protein<sup>19</sup> that, having a large molecular mass, suffers from similar problems of fast nuclear relaxation as paramagnetic systems do.

Here, we determine to what extent  $^{13}\text{C}$  2D scalar (CT-COSY, COCAMQ) and dipolar (NOESY) correlation experiments can improve detection and assignment of resonances in paramagnetic systems. To best exploit the potential of this approach, we have implemented homodecoupling of carbonyl from aliphatic signals, and vice versa, to simplify the spectra and alleviate the problem of signal overlap. The experiments can be acquired on a standard spectrometer configured for triple resonance experiments but benefit significantly from the use of probeheads optimized for  $^{13}\text{C}$  detection.

The approach is applied to the monomeric analogue of superoxide dismutase (SOD).<sup>21</sup> This copper, zinc-containing enzyme catalyzes dismutation of superoxide to  $\text{O}_2$  and  $\text{H}_2\text{O}$ . The copper ion, present as copper(II) in its resting state, switches to copper(I) during the catalytic cycle. Extensive literature is available on superoxide dismutase, including the solution structure of the enzyme<sup>22</sup> and of several mutants.<sup>23,24</sup> However, all the high-resolution NMR studies either addressed only the reduced form of the protein or resorted to metal substitution<sup>25</sup> for assigning resonances in the proximity of the copper ion.

We would like here to address to what extent  $^{13}\text{C}$  direct experiments can allow detection and assignment of broad signals in paramagnetic proteins. This  $^{13}\text{C}$ -based methodology could contribute to the study of metal-containing enzymes when the metal is paramagnetic as well as of large molecules for which the rotational correlation time makes  $^1\text{H}$  relaxation unfavorable.

## Materials and Methods

**Sample Preparation.** The  $^{13}\text{C}$ ,  $^{15}\text{N}$ -labeled monomeric mutant F50E/G51E/E133Q of superoxide dismutase was expressed and purified as previously reported.<sup>26,27</sup> The protein concentration in the final NMR samples was about 1.5 mM. The buffer was 20 mM phosphate at pH 5.0. Two samples were necessary: one with the oxidized and one with the reduced form of the protein. The former was maintained in the oxidized state by oxygen. The latter was reduced under anaerobic conditions with sodium ascorbate. 10%  $\text{D}_2\text{O}$  was added for the lock signal. All the spectra detailed below were recorded at 298 K.

**NMR Experiments.**  $^{13}\text{C}$  direct detection experiments were carried out with three different instruments. Two were 16.4 T Bruker AVANCE 700 spectrometers, operating at 700.13 MHz for  $^1\text{H}$  and 176.08 MHz for  $^{13}\text{C}$ . One was equipped with a TXI  $^1\text{H}$   $\{^{13}\text{C}, ^{15}\text{N}\}$  probe and the other with a TXO  $^{13}\text{C}, ^{15}\text{N}$   $\{^1\text{H}\}$  probe. The third instrument was a 11.7 T Bruker AVANCE 500 spectrometer, operating at 500.23 MHz for  $^1\text{H}$  and 125.79 MHz for  $^{13}\text{C}$  and equipped with a DUAL  $^{13}\text{C}$   $\{^1\text{H}\}$  CryoProbe. The  $^{13}\text{C}$ ,  $^{15}\text{N}$ , and  $^1\text{H}$  carriers were set at 98, 120, and 4.7 ppm, respectively, and the recycle delay was 0.9–1.1 s, unless otherwise specified. At 11.7 T, the experiments were performed without  $^{15}\text{N}$  decoupling. Each experiment was run at the different spectrometers with the same parameters, except for the number of scans and for machine-related parameters.

Control  $^1\text{H}$ – $^{15}\text{N}$  HSQC experiments to check sample integrity were acquired with standard parameters.<sup>28</sup> The  $^{13}\text{C}$ – $^{13}\text{C}$  CT-COSY experiments<sup>29</sup> were acquired with a spectral width of 200 ppm in both dimensions, with  $4096 \times 200$  data points, with a CT delay of 8.3 ms and with 64 scans per increment. The  $90^\circ$  pulses were hard square pulses, while the  $180^\circ$  pulse was applied as an adiabatic smoothed chirp<sup>30</sup> (total sweep width of 60 kHz, 0.5 ms length, 10% smoothing). The phase-roll effect induced by the use of an adiabatic pulse does not affect the quality of the spectra as they were processed in magnitude mode. Composite pulse decoupling on  $^1\text{H}$  and  $^{15}\text{N}$  was applied during the whole duration of the experiment and during acquisition with a RF field strength of 3.12 kHz for  $^1\text{H}$  (waltz) and 1.4 kHz for  $^{15}\text{N}$  (garp), respectively.  $^{15}\text{N}$  composite pulse decoupling was not applied when experiments were acquired on the DUAL  $^{13}\text{C}$   $\{^1\text{H}\}$  CryoProbe.

The  $^{13}\text{C}$ – $^{13}\text{C}$  COCAMQ experiment was acquired with a similar approach as the HMQC experiment<sup>31</sup> where the  $^1\text{H}$  pulses are substituted with  $^{13}\text{C}'$  semi-selective pulses and the heteronuclear pulses are substituted with  $^{13}\text{C}\alpha$  semi-selective pulses. The  $90^\circ$  pulses were Gaussian cascades (Q5) of 409 and 333  $\mu\text{s}$  at 11.7 and 16.4 T, respectively. The  $180^\circ$   $\text{C}'$  pulse was a square pulse and was set as short as possible to have zero inversion on the  $\text{C}\alpha$  (56  $\mu\text{s}$  at 11.7 T, 40  $\mu\text{s}$  at 16.4 T). The  $^{13}\text{C}$  carrier was set to 178 ppm to pulse on  $\text{C}'$ , and frequency jumped to 50 ppm when pulsing on  $\text{C}\alpha$ . The sweep width was 50 ppm in the two dimensions, and  $1024 \times 200$  points were acquired in the direct and indirect dimensions, respectively. The experiment was acquired once with the coherence transfer delay slightly shorter than  $1/2J_{\text{C}\alpha-\text{C}'}$  (8.3 ms) and a second time with the delay significantly shorter than  $1/2J_{\text{C}\alpha-\text{C}'}$  (5.5 ms) to minimize relaxation losses during this interval, even if at the expense of the transfer efficiency. The relaxation delay in the second case was also shortened to 800 ms. Decoupling of  $^1\text{H}$  and  $^{15}\text{N}$  was achieved with a  $180^\circ$  hard pulse during the indirect dimension and with composite pulse decou-

- (10) Arnesano, F.; Banci, L.; Bertini, I.; Mangani, S.; Thompson, A. R. *Proc. Natl. Acad. Sci. U.S.A.* **2003**, *100*, 3814–3819.
- (11) Arnesano, F.; Banci, L.; Bertini, I.; Felli, I. C.; Luchinat, C.; Thompson, A. R. *J. Am. Chem. Soc.* **2003**, *125*, 7200–7208.
- (12) Kolczak, U.; Salgado, J.; Siegal, G.; Saraste, M.; Canters, G. W. *Biospectroscopy* **1999**, *5*, S19–S32.
- (13) Serber, Z.; Richter, C.; Moskau, D.; Boehlen, J.-M.; Gerfin, T.; Marek, D.; Haeblerli, M.; Baselgia, L.; Laukien, F.; Stern, A. S.; Hoch, J. C.; Doetsch, V. *J. Am. Chem. Soc.* **2000**, *122*, 3554–3555.
- (14) Serber, Z.; Richter, C.; Dötsch, V. *ChemBioChem* **2001**, *2*, 247–251.
- (15) Bertini, I.; Lee, Y.-M.; Luchinat, C.; Piccioli, M.; Poggi, L. *ChemBioChem* **2001**, *2*, 550–558.
- (16) Pochapsky, T. C.; Pochapsky, S. S.; Ju, T.; Mo, H.; Al-Mjeni, F.; Maroney, M. J. *Nat. Struct. Biol.* **2002**, *9*, 966–972.
- (17) Machonkin, T. E.; Westler, W. M.; Markley, J. L. *J. Am. Chem. Soc.* **2002**, *124*, 3204–3205.
- (18) Kostic, M.; Pochapsky, S. S.; Pochapsky, T. C. *J. Am. Chem. Soc.* **2002**, *124*, 9054–9055.
- (19) Eletsky, A.; Moreira, O.; Kovacs, H.; Pervushin, K. *J. Biomol. NMR* **2003**, *26*, 167–179.
- (20) Pervushin, K.; Eletsky, A. *J. Biomol. NMR* **2003**, *25*, 147–152.
- (21) Bertini, I.; Piccioli, M.; Viezzoli, M. S.; Chiu, C. Y.; Mullenbach, G. T. *Eur. Biophys. J.* **1994**, *23*, 167–176.
- (22) Banci, L.; Bertini, I.; Cramaro, F.; Del Conte, R.; Viezzoli, M. S. *Eur. J. Biochem.* **2002**, *269*, 1905–1915.
- (23) Banci, L.; Benedetto, M.; Bertini, I.; Del Conte, R.; Piccioli, M.; Viezzoli, M. S. *Biochemistry* **1998**, *37*, 11780–11791.
- (24) Banci, L.; Bertini, I.; Del Conte, R.; Mangani, S.; Viezzoli, M. S.; Fadin, R. *J. Biol. Inorg. Chem.* **1999**, *4*, 795–803.
- (25) Bertini, I.; Luchinat, C.; Piccioli, M. *Prog. Nucl. Magn. Reson. Spectrosc.* **1994**, *26*, 91–141.

- (26) Banci, L.; Bertini, I.; Cramaro, F.; Del Conte, R.; Rosato, A.; Viezzoli, M. S. *Biochemistry* **2000**, *39*, 9108–9118.
- (27) Banci, L.; Benedetto, M.; Bertini, I.; Del Conte, R.; Piccioli, M.; Richert, T.; Viezzoli, M. S. *Magn. Reson. Chem.* **1997**, *35*, 845–853.
- (28) Kay, L. E.; Keifer, P.; Saarinen, T. *J. Am. Chem. Soc.* **1992**, *114*, 10663–10665.
- (29) Rance, M.; Wagner, G.; Sorensen, O. W.; Wüthrich, K.; Ernst, R. R. *J. Magn. Reson.* **1984**, *59*, 250–261.
- (30) Boehlen, J.-M.; Bodenhausen, G. *J. Magn. Reson., Ser. A* **1993**, *102*, 293–301.
- (31) Bax, A.; Griffey, R. H.; Hawkins, B. L. *J. Magn. Reson.* **1983**, *55*, 301–315.

pling during acquisition with the parameters mentioned for the <sup>13</sup>C–<sup>13</sup>C CT-COSY experiment.

The <sup>13</sup>C–<sup>13</sup>C NOESY experiments<sup>32</sup> were acquired at 11.7 T using a DUAL <sup>13</sup>C{<sup>1</sup>H} CryoProbe with a spectral width of 200 ppm in both dimensions. Three experiments were acquired with different experimental conditions to enhance fast-relaxing signals. The mixing times used were 200, 50, and 25 ms with relaxation delays of 580, 280, and 220 ms, respectively. In all the experiments, 4096 data points for acquisition were acquired, while the number of increments were set to 256, 128, and 96, with 576, 6144, and 8192 transients per increment, respectively. <sup>1</sup>H decoupling was applied during evolution and during acquisition with an RF field strength of 3.12 kHz.

Band-selective homodecoupling of <sup>13</sup>C' from <sup>13</sup>Cα and vice versa was first set up on 1D experiments and then implemented in the <sup>13</sup>C–<sup>13</sup>C COCAMQ and <sup>13</sup>C–<sup>13</sup>C CT-COSY experiments. Adiabatic chirp pulses<sup>30</sup> with 10-ms pulse length, 25% smoothing, and sweep from low to high field were used. The sweep width was chosen 20% larger than the bandwidth to be covered by decoupling. The RF field strength was calculated according to the sweep width and the homodecoupling duty-cycle (hdduty hereafter) in every experiment. A p5m4<sup>33,34</sup> supercycle was chosen for composite pulse decoupling. The hdduty was set to ca. 20% as a compromise between giving up signal-to-noise (sampling points) and using not too high RF power (probe ringdown, sidebands; cf. infra). This generated a “DANTE-like” pulse train with irradiation sidebands occurring at multiples of the reciprocal of the interpulse delay. Setting the sweep width and placing the carrier frequency therefore needed some care to avoid irradiation of the signals of interest by sidebands of the band-selective homodecoupling. Besides the Bloch–Siegert shift, band-selective homodecoupling using composite pulse decoupling with cyclic schemes induced decoupling sidebands around the signals of interest. The intensity of the induced sidebands increased with the strength of the decoupling RF field and, therefore, not using too much decoupling power was desirable (i.e., using higher hdduty). Changing the phase of the sidebands in a controlled manner by starting the decoupling sequence at different times prior to acquisition permitted canceling them to a good extent.<sup>35–37</sup> Removing the coupling of two coupled spins with (band-selective) homodecoupling allowed an increase in the signal-to-noise ratio (S/N). For a complete decoupling, one would expect a factor of 2 gain. However, during switching from observe to transmit and irradiation for decoupling no sampling points can be taken. Therefore the S/N gain depends on the hdduty:  $S/N(\text{HD}) = 2S/N \cdot \sqrt{1 - \frac{\text{hdduty}}{100}}$ , e.g., a factor of 1.79 using a hdduty of 20% is expected. In practice, this factor is smaller.

In the decoupled spectra, the <sup>13</sup>C carrier for acquisition was set between the spectral part of interest and the decoupling offset. Strip transformation was then used for processing only the spectral region of interest at high resolution.

All the <sup>13</sup>C 2D sequences used and the details for their implementation are reported in the Supporting Information.

**Relaxation Equations.** Nuclear longitudinal ( $R_1$ ) and transverse ( $R_2$ ) relaxation rates due to the dipolar coupling with a paramagnetic center are strongly dependent on the electronic relaxation time according to the following equations:<sup>38–41</sup>

$$R_{1M} = \frac{2}{15} \left( \frac{\mu_0}{4\pi} \right)^2 \frac{\gamma_1^2 g_e^2 \mu_B^2 S(S+1)}{r^6} \times \left[ \frac{\tau_c}{1 + (\omega_1 - \omega_s)^2 \tau_c^2} + \frac{3\tau_c}{1 + \omega_1^2 \tau_c^2} + \frac{6\tau_c}{1 + (\omega_1 + \omega_s)^2 \tau_c^2} \right] + \frac{2}{5} \left( \frac{\mu_0}{4\pi} \right)^2 \frac{\omega_1^2 g_e^4 \mu_B^4 S^2(S+1)^2}{(3kT)^2 r^6} \frac{3\tau_r}{1 + \omega_1^2 \tau_r^2} \quad (1)$$

$$R_{2M} = \frac{1}{15} \left( \frac{\mu_0}{4\pi} \right)^2 \frac{\gamma_1^2 g_e^2 \mu_B^2 S(S+1)}{r^6} \times \left[ 4\tau_c + \frac{\tau_c}{1 + (\omega_1 - \omega_s)^2 \tau_c^2} + \frac{3\tau_c}{1 + \omega_1^2 \tau_c^2} + \frac{6\tau_c}{1 + (\omega_1 + \omega_s)^2 \tau_c^2} + \frac{6\tau_c}{1 + \omega_s^2 \tau_c^2} \right] + \frac{1}{5} \left( \frac{\mu_0}{4\pi} \right)^2 \frac{\omega_1^2 g_e^4 \mu_B^4 S^2(S+1)^2}{(3kT)^2 r^6} \left( 4\tau_r + \frac{3\tau_r}{1 + \omega_1^2 \tau_r^2} \right) \quad (2)$$

where the first term of each equation describes the contribution from the electron spin–nuclear spin dipolar interaction and the second term describes the Curie contribution, both dependent on the electron–nucleus distance.  $\gamma_1$  is the nuclear gyromagnetic ratio,  $g_e$  is the free electron g factor,  $S$  is the quantum number associated to the electron spin,  $r$  is the electron–nucleus distance,  $\omega_1$  and  $\omega_s$  are the Larmor frequencies of the nucleus and of the electron, respectively,  $\tau_r$  is the rotational correlation time,  $\tau_s$  is the electronic correlation time,  $\tau_c$  is the effective correlation time ( $1/\tau_c = 1/\tau_s + 1/\tau_r$ ), and the remaining symbols have their usual meaning. The contact contribution to relaxation induced by the paramagnetic center is not included in the above equations because it is not further discussed in the text.

These equations were used to calculate the paramagnetic contribution to longitudinal and transverse relaxation rates, taking the value for the different correlation times from previous estimates.<sup>26,42</sup>

## Results and Discussion

**Assignment of the Diamagnetic Signals.** The general strategy here is that of assigning the <sup>13</sup>C nuclei through the classic approach applicable to the diamagnetic reduced protein. This step is not necessary in general, but it may represent a shortcut, especially when the assignment is already available.<sup>27</sup> The rationale is that copper(II) magnetic anisotropy is small; thus, the pseudocontact contributions to the chemical shift are small, and they have a minor affect only on the residues very close to the metal center. Therefore, a large proportion of the assigned <sup>13</sup>C lines can be recognized in the paramagnetic sample spectra. The available assignment of reduced SOD comprises 88% H, 95% amide NH, 98% C', and 98% Cα.<sup>23,27</sup> With a minimal set of double and triple resonance experiments on the oxidized paramagnetic sample, we were able to transfer a large proportion of the assignments available for reduced SOD to oxidized SOD. With this approach, we could identify most of the <sup>13</sup>C nuclei at distances of more than 11 Å from the copper-(II) ion. The <sup>13</sup>C nuclei at a distance shorter than 11 Å could not be detected at this stage. In some cases, signal overlap prevented a safe transfer of the assignment from the reduced to the oxidized form of SOD, and we omitted these resonances in the subsequent analysis.

Because we were interested in the assignment of the residues that could not be assigned by using the standard procedure, we identified all the residues within the 11 Å threshold (Figure 1)

(32) Macura, S.; Wüthrich, K.; Ernst, R. R. *J. Magn. Reson.* **1982**, *47*, 351–357.  
 (33) Tycko, R.; Pines, A.; Guckenheimer, J. *J. Chem. Phys.* **1985**, *83*, 2775–2802.  
 (34) Fujiwara, T.; Nagayama, J. *J. Magn. Reson.* **1988**, *77*, 53–64.  
 (35) Hammarstroem, A.; Otting G. *J. Am. Chem. Soc.* **1994**, *116*, 8847–8848.  
 (36) Kupce, E.; Boyd, J.; Freeman, R. *J. Magn. Reson., Ser. B* **1995**, *106*, 300–303.  
 (37) Weigelt, J.; Hammarstroem, A.; Bermel, W.; Otting G. *J. Magn. Reson., Ser. B* **1996**, *110*, 219–224.  
 (38) Solomon, I. *Phys. Rev.* **1955**, *99*, 559–565.  
 (39) Bloembergen, N. *J. Chem. Phys.* **1957**, *27*, 572–573.  
 (40) Solomon, I.; Bloembergen, N. *J. Chem. Phys.* **1956**, *25*, 261–266.  
 (41) Gueron, M. *J. Magn. Reson.* **1975**, *19*, 58–66.

(42) Bertini, I.; Banci, L.; Brown, R. D., III; Koenig, S. H.; Luchinat, C. *Inorg. Chem.* **1988**, *27*, 951–953.



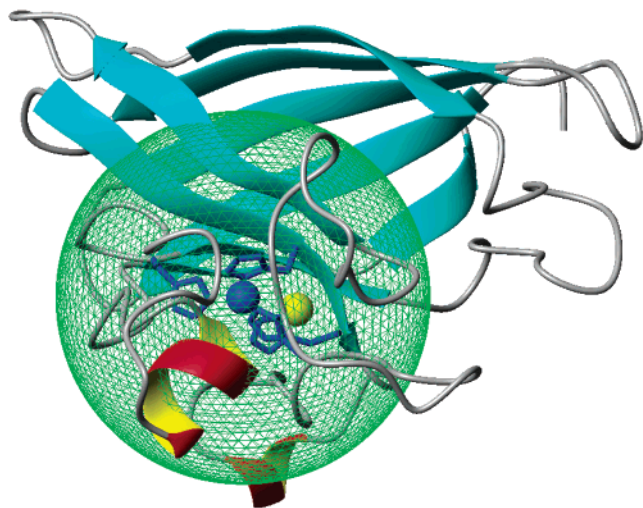


**Figure 1.** Display of the solution structure of monomeric SOD (PDB id IBA9).<sup>23</sup> The 11 Å radius sphere represents the region for which <sup>1</sup>H NMR signals are not detectable due to Cu(II)-induced paramagnetic broadening.

in the available solution structure family of the reduced form.<sup>23</sup> Without considering those residues for which the NH was assigned in the oxidized form and those for which the assignment was not available from the reduced maps, we systematically searched for the hyperfine broadened signals in <sup>13</sup>C–<sup>13</sup>C spectra.

**Detection of Paramagnetic Signals.** The 2D <sup>13</sup>C direct detection experiments selected for extending the assignment of oxidized SOD were 2D <sup>13</sup>C–<sup>13</sup>C CT-COSY, <sup>13</sup>C–<sup>13</sup>C COCAMQ, and <sup>13</sup>C–<sup>13</sup>C NOESY.

<sup>13</sup>C–<sup>13</sup>C CT-COSY has been shown to be a valuable experiment to detect correlations between fast-relaxing spins.<sup>11,17</sup> The experiment allowed us to detect one-bond scalar correlations with good sensitivity. To achieve a compromise between detecting fast-relaxing signals and still obtaining good quality spectra, it was necessary to keep the delays during which magnetization is transverse as short as possible but still compatible with achieving coherence transfer. We chose to optimize detection of all one-bond correlations; thus, we set the CT delay at 8.3 ms. This experiment allowed us to obtain information over large spectral widths. However, severe problems of signal overlap occurred in crowded spectral regions. Therefore, the <sup>13</sup>C–<sup>13</sup>C CT COSY experiment proved particularly useful for identifying correlations in regions of the spectra that are not too crowded. In this respect, a very clean and interesting region of the spectra is the one containing Cβ–Cγ correlations of aromatic residues, which are often involved in metal binding or are relevant for defining hydrophobic interactions; thus, information on their spin systems may be crucial for defining important structural details. In the reduced form of the protein, the Cβ–Cγ correlation of the 12 aromatic residues present in the protein are well-resolved and readily assigned (data not shown). In the oxidized form of the protein, the Cβ–Cγ of all the aromatic residues in SOD >7 Å from the paramagnetic center can be detected (Figure 2A). The Cu(II) ligand spin systems (Cu–Cγ distance of 3.0–4.1 Å) as well as the correlation for Cβ–Cγ of Phe 45 (Cu–Cγ distance of 6.8 Å) are missing.

The <sup>13</sup>C–<sup>13</sup>C NOESY experiment can be used to detect correlations between nuclei that are close in space.<sup>43</sup> The transfer

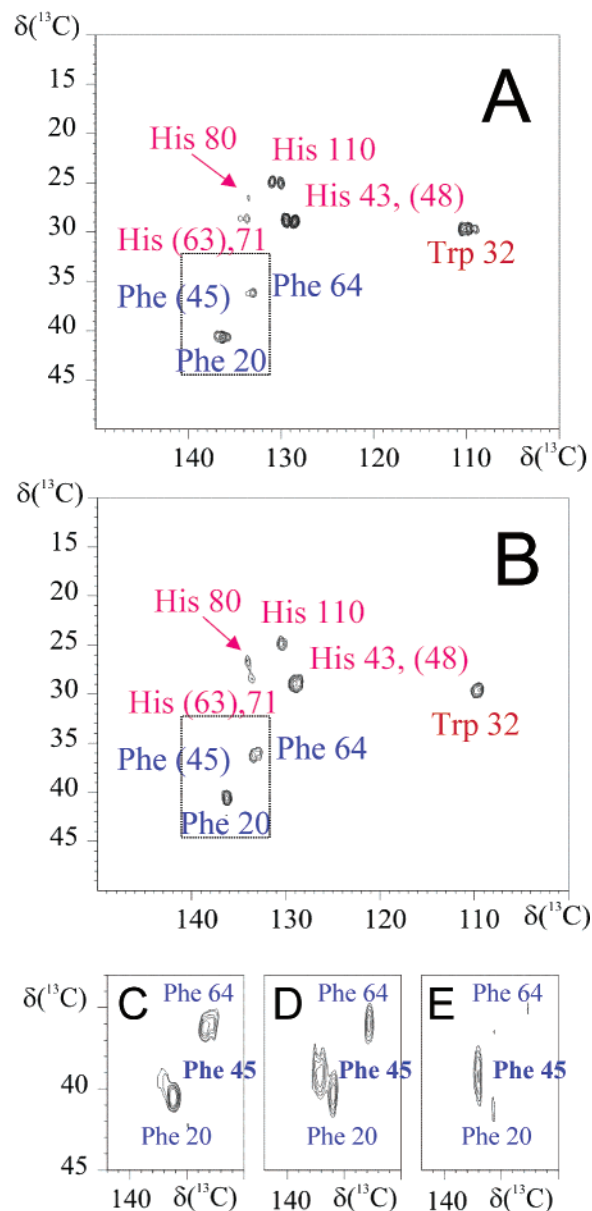


**Figure 2.** Part of 2D <sup>13</sup>C–<sup>13</sup>C spectra containing Cβ–Cγ correlations of aromatic residues acquired at 11.7 T on oxidized SOD. The <sup>13</sup>C–<sup>13</sup>C CT-COSY (A) and the <sup>13</sup>C–<sup>13</sup>C NOESY (B) are shown. The correlation of Phe 45 can be detected only through the <sup>13</sup>C–<sup>13</sup>C NOESY experiments. In panel C, an expansion of panel B is shown with a lower threshold to detect the Phe 45 Cβ–Cγ correlation. In panels D and E, the results obtained by pushing the experimental conditions to enhance fast-relaxing signals are shown. The mixing times of the NOESY experiments reported in panels B, C, and D are 200, 50, and 25 ms, respectively. Residues that were not detected have the residue number in brackets.

efficiency of this experiment, at least in the case of monomeric SOD (16 kDa), is definitely lower than that of the <sup>13</sup>C–<sup>13</sup>C CT COSY experiment, but it is enough to be able to detect at least one-bond correlations. For this reason, the experiment can turn out very advantageous to detect correlations between fast-relaxing nuclei, especially when transverse contributions to relaxation are the dominant ones. In fact, NOESY experiments depend on longitudinal relaxation, which is much smaller than transverse relaxation in copper(II) systems at high magnetic fields. Several <sup>13</sup>C–<sup>13</sup>C NOESY experiments were acquired at

(43) Fisher, M. W. F.; Zeng, L.; Zuiderweg, E. R. P. *J. Am. Chem. Soc.* **1996**, *118*, 12457–12458.

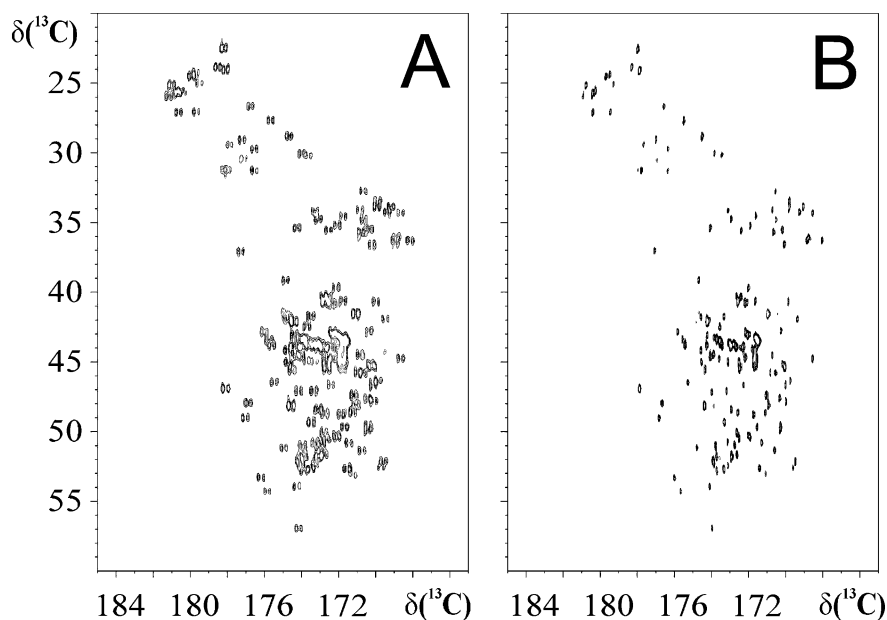


**Figure 3.** <sup>13</sup>C–<sup>13</sup>C COCAMQ spectra recorded at 16.4 T on oxidized SOD. Comparison of the <sup>13</sup>C–<sup>13</sup>C COCAMQ spectrum acquired with a TXO probehead without (A) and with (B) band-selective homodecoupling of C $\alpha$  signals during acquisition.

11.7 T, using a DUAL <sup>13</sup>C{<sup>1</sup>H} CryoProbe, in which the mixing and relaxation delays were gradually optimized for <sup>13</sup>C signals that are fast-relaxing to pick up some of the correlations that were lost in the scalar experiments. As an example, Figure 2 reports the region containing C $\beta$ –C $\gamma$  correlations of aromatic residues, including that of Phe 45 (Figure 2B). In the insets 2C–E, the same portion of the spectra recorded with three different experimental conditions to progressively enhance fast-relaxing signal detection are shown. This shows that the NOESY experiment can prove very useful when transverse relaxation rates are affected more dramatically than longitudinal ones by the paramagnetic interactions, as is this case.

For the assignment of the C'–C $\alpha$  connectivities in paramagnetic systems, <sup>13</sup>C–<sup>13</sup>C multiple quantum (MQ) experiments were recently proposed.<sup>18</sup> In the present case, we decided to acquire C' and have C $\alpha$  in the indirect dimension to minimize evolution of the additional C $\alpha$ –C $\beta$  couplings (the <sup>13</sup>C–<sup>13</sup>C COCAMQ experiments). The 180° pulse in the middle of the evolution time was applied as a short frequency-matched square pulse to avoid additional delays and to minimize phase corrections. One-bond correlations between carbonyl and aliphatic carbons are identified through this experiment and include backbone C'–C $\alpha$  correlations as well as side chain CO–C $\beta/\gamma$  peaks of Asp, Asn, Glu, and Gln residues. The resulting spectrum is reported in Figure 3A. The pure absorption lineshape of the peaks in this experiment makes it the preferred choice for detection of correlations between carbonyl and aliphatic carbons compared to the <sup>13</sup>C–<sup>13</sup>C CT-COSY experiment.

As a result of the analysis of the <sup>13</sup>C–<sup>13</sup>C CT-COSY and COCAMQ maps, we were able to identify a number of C'–C $\alpha$  cross-peaks (Table 1) for which the NH could not be detected in <sup>1</sup>H–<sup>15</sup>N correlation spectra. The correlations that could only be identified either by the use of <sup>13</sup>C direct detection probes (TXO and DUAL <sup>13</sup>C{<sup>1</sup>H} CryoProbe) and/or by tailoring the experiment for paramagnetic signals are indicated.

However, a severe problem of signal overlap is evident in the <sup>13</sup>C–<sup>13</sup>C COCAMQ and can be removed by <sup>13</sup>C band-

**Table 1.** Residues for Which the C'–C $\alpha$  Connectivity Was Identified in the <sup>13</sup>C Observed 2D Experiments<sup>a</sup>

residue no.	C'–Cu(II) (Å)	C $\alpha$ –Cu(II) (Å)	residue no.	C'–Cu(II) (Å)	C $\alpha$ –Cu(II) (Å)
<i>b</i> 44	5.3–6.0	6.0–6.6	121	9.8–10.2	9.5–9.8
<i>b</i> 45	4.6–5.7	4.9–6.4	123	8.7–9.7	9.5–10.5
<i>b</i> 46	4.3–5.1	4.0–4.7	124	9.1–10.2	7.7–8.8
<i>b</i> 47	5.6–6.1	5.9–6.6	133	9.6–11.4	10.3–12.3
<i>b</i> 48 <sup>c</sup>	7.3–7.6	5.8–6.1	134	9.5–11.3	9.9–11.6
62	5.7–7.0	6.0–7.8	<i>b</i> 136	6.4–8.4	7.9–9.9
64	8.8–10.0	8.2–9.2	<i>b</i> 137	5.2–6.8	5.2–6.9
72	10.2–11.5	10.5–11.9	139 <sup>c</sup>	8.8–10.0	9.1–10.2
80	10.2–11.9	9.8–11.4	<i>b</i> 141	7.8–8.6	8.5–9.5
<i>b</i> 83	8.2–8.9	7.4–8.2	<i>b</i> 142	7.4–8.4	8.2–9.3
85	8.0–8.8	8.6–9.5	<i>b</i> 143	7.9–9.1	6.6–7.8
<i>b</i> 86	10.0–11.0	8.9–9.8	144	9.7–11.2	9.5–10.8
116	7.6–9.0	8.9–10.2	145 <sup>c</sup>	8.2–9.9	9.2–10.9
<i>b</i> 118	4.2–5.9	4.7–6.0	146 <sup>c</sup>	9.6–11.2	8.4–10.0
<i>b</i> 119	5.2–6.8	5.2–7.2	147	10.6–12.4	10.6–12.3
<i>b</i> 120	7.4–7.8	5.9–6.4			

<sup>a</sup> The corresponding NH cross-peak in the <sup>1</sup>H–<sup>15</sup>N HSQC spectra could not be detected because it was within 11 Å from the copper(II) ion. <sup>b</sup> Those cases for which either a probehead optimized for <sup>13</sup>C detection and/or tailoring of the experiment were necessary to clearly detect the signal. The distances are the minimum and maximum nucleus–Cu(II) distances determined in the family of 35 structures representing the solution structure of monomeric SOD.<sup>23</sup> <sup>c</sup> Not firmly assigned for partial overlap.

selective homodecoupling. Figure 3 compares two <sup>13</sup>C–<sup>13</sup>C COCAMQ spectra acquired without (Figure 3A) and with (Figure 3B) homodecoupling but otherwise using the same parameters. The spectra show that the C'–C $\alpha$  coupling has been removed. Therefore, a much better resolution is achieved, and 121 backbone correlations as well as 25 side-chain correlations are now resolved and easily identified, compared to 65 backbone and 19 side-chain correlations resolved in the coupled spectrum.

### Discussion

Cu(II) is a d<sup>9</sup> metal ion with one unpaired electron. The magnetic electron–nucleus coupling (hyperfine interaction) causes dramatic effects on chemical shifts and relaxation properties of the nuclei nearby. For copper(II) in particular, the

**Table 2.** Relaxation Rates ( $s^{-1}$ ) Calculated for  $^1\text{H}$ ,  $^{13}\text{C}$ , and  $^{15}\text{N}$  Nuclei (N) at Various Distances from a Copper(II) Ion at 16.4 T According to Eqs 1 and 2, Assuming a  $\tau_S$  Value of  $2.2 \times 10^{-9} s^{42}$  and a  $\tau_r$  Value of  $9.2 \times 10^{-9} s^{26}$ 

Cu(II)-N (Å)	$^1\text{H}$			$^{13}\text{C}$			$^{15}\text{N}$		
	$R_1$	$R_2$	$\Delta\nu$	$R_1$	$R_2$	$\Delta\nu$	$R_1$	$R_2$	$\Delta\nu$
3	2910.0	122517.4	38998.5	2348.7	8832.0	2811.3	1138.8	1811.7	576.7
4	517.9	21805.5	6940.9	418.0	1571.9	500.4	202.7	322.4	102.6
5	135.8	5716.2	1819.5	109.6	412.1	131.2	53.1	84.5	26.9
6	45.5	1914.3	609.3	36.7	138.0	44.9	17.8	28.3	9.0
7	18.0	759.1	241.6	14.6	54.7	17.4	7.0	11.2	3.6
8	8.1	340.7	108.4	6.5	24.6	7.8	3.2	5.0	1.6
9	4.0	168.1	53.5	3.2	12.1	3.8	1.5	2.5	0.8
10	2.1	89.3	28.4	1.7	6.4	2.0	0.8	1.3	0.4
11	1.2	50.4	16.0	1.0	3.6	1.2	0.5	0.7	0.2

effect on nuclear relaxation rates is dramatic while the effect on the chemical shift is small, except for nuclei experiencing contact contribution.

In the case of copper(II) SOD, the electronic correlation time has been measured through NMRD and is 2.2 ns.<sup>8</sup> Using this value, together with the overall rotational correlation time measured through  $^{15}\text{N}$  relaxation in the diamagnetic reduced form (9.2 ns),<sup>26</sup> we can calculate the paramagnetic contributions to relaxation rates that are reported in Table 2, calculated with eqs 1 and 2 (see Materials and Methods section). The table clearly shows that significant contributions to  $^1\text{H}$  relaxation ( $>20$  Hz), adding to the diamagnetic linewidths, already occur at 10 Å from the paramagnetic center, whereas a comparable contribution to  $^{13}\text{C}$  and  $^{15}\text{N}$  nuclei arises only at 6 and 5 Å from the paramagnetic center, respectively. Therefore, heteronuclear spectroscopy is much more promising than proton spectroscopy to detect fast-relaxing signals, despite the lower sensitivity.

Proton signals with very large linewidths can be detected when they are shifted out of the crowded diamagnetic region and fall in clean regions of the spectra.<sup>44–51</sup> The small shifts and the very large relaxation rates, characteristic of Cu(II)-containing systems, should be used as guidelines for the choice and optimization of the experiments. In the present case, the signals experiencing contact contribution are broad beyond detectable limits, while a significant number of residues that experience large dipolar effects on relaxation fall in the diamagnetic spectral region. As already shown for CopC,<sup>11</sup> another type II Cu(II) protein, shifting from  $^1\text{H}$  to  $^{13}\text{C}$  detection allowed us to narrow the blind sphere from 11 to 6 Å, despite the use of a standard triple resonance spectrometer optimized for  $^1\text{H}$  sensitivity. The detection limit can be further pushed by the use of probes optimized for  $^{13}\text{C}$  detection as well as by optimization of experiments. On copper(II) SOD, we have extended the set of experiments used in the CopC case to include also  $^{13}\text{C}$ – $^{13}\text{C}$  COCAMQ and  $^{13}\text{C}$ – $^{13}\text{C}$  NOESY, and we have

optimized them also on a TXO and on a DUAL  $^{13}\text{C}\{^1\text{H}\}$  CryoProbe.  $^{13}\text{C}$  signals as close as 4 Å from the copper(II) can be detected if they do not experience Fermi contact contribution. Apparently, the latter contribution broadens the lines beyond detectable limits.

The results show that the  $^{13}\text{C}$ – $^{13}\text{C}$  CT-COSY experiment is very useful to detect one-bond correlations over a large spectral window (carbonyl, aromatic, and aliphatic carbons) in a single experiment. The intrinsic problem of COSY lineshapes, however, prevents good resolution in crowded regions.  $^{13}\text{C}$ – $^{13}\text{C}$  COCAMQ, still in the class of scalar experiments, allows us to get better quality spectra in the  $C'$ – $C\alpha$  region thanks to the better lineshape, without significant losses in relaxation. This experiment is thus preferred over the  $^{13}\text{C}$ – $^{13}\text{C}$  CT-COSY to detect  $C'$ – $C\alpha$  correlations.

Coherence transfer mechanisms become less effective as the linewidths of the signals approach the value of the scalar coupling constant used for the transfer. In case of one-bond carbon–carbon couplings, the  $^1J_{CC}$  is fairly large (35–55 Hz), but the inspection of Table 2 shows that the paramagnetic  $R_2$  contributions do approach and overcome this range. This means that to detect such broad signals alternative approaches should be used. Inspection of Table 2 also shows that the paramagnetic contribution to relaxation is much less effective on longitudinal rates (compared to transverse rates). Therefore, experiments in which magnetization is stored along the  $z$  axis should be affected to a minor extent by paramagnetic relaxation. This is the case of  $^{13}\text{C}$ – $^{13}\text{C}$  NOESY experiments. We would like to point out here that with the availability of more sensitive probes for  $^{13}\text{C}$  detection the use of  $^{13}\text{C}$ – $^{13}\text{C}$  NOESY can become of strategic importance in all cases in which transverse relaxation is prohibitively fast while longitudinal relaxation is still acceptable. This is actually a common behavior typical of both large systems and paramagnetic systems.

The other pressing problem of 2D  $^{13}\text{C}$ – $^{13}\text{C}$  direct detection experiments is the large amount of carbon–carbon coupling constants that complicate the spectra. They are very useful to achieve coherence transfer and also potentially useful, provided they can be resolved, for detection of residual dipolar couplings induced by high magnetic fields or by external media. However, they significantly reduce the sensitivity of numerous experiments and prohibit spectral interpretation due to increased signal overlap. Band-selective homodecoupling can, in part, solve the problem. As shown above, it is possible to decouple  $C'$  from  $C\alpha$  (and  $C\beta$  eventually) and vice versa, decoupling the aliphatic carbons from carbonyls. This is sufficient to quench all the relevant carbon–carbon couplings in the acquisition dimension

- (44) Kalverda, A. P.; Salgado, J.; Dennison, C.; Canters, G. W. *Biochemistry* **1996**, *35*, 3085–3092.
- (45) Luchinat, C.; Soriano, A.; Djinic-Carugo, K.; Saraste, M.; Malmström, B. G.; Bertini, I. *J. Am. Chem. Soc.* **1997**, *119*, 11023–11027.
- (46) Salgado, J.; Warmerdam, G.; Bubacco, L.; Canters, G. W. *Biochemistry* **1998**, *37*, 7378–7389.
- (47) Bertini, I.; Ciurli, S.; Dikiy, A.; Gasanov, R.; Luchinat, C.; Martini, G.; Safarov, N. *J. Am. Chem. Soc.* **1999**, *121*, 2037–2046.
- (48) Bubacco, L.; Salgado, J.; Tepper, A. W.; Vijgenboom, E.; Canters, G. W. *FEBS Lett.* **1999**, *442*, 215–220.
- (49) Bertini, I.; Fernández, C. O.; Karlsson, B. G.; Leckner, J.; Luchinat, C.; Malmström, B. G.; Nersissian, A. M.; Pierattelli, R.; Shipp, E.; Valentine, J. S.; Vila, A. J. *J. Am. Chem. Soc.* **2000**, *122*, 3701–3707.
- (50) Dennison, C.; Oda, K.; Kohzuma, T. *Chem. Commun.* **2000**, 751–752.
- (51) Donaire, A.; Jimenez, B.; Fernandez, C. O.; Pierattelli, R.; Niizeki, T.; Moratal, J. M.; Hall, J. F.; Kohzuma, T.; Hasnain, S. S.; Vila, A. J. *J. Am. Chem. Soc.* **2002**, *124*, 13698–13708.

of <sup>13</sup>C–<sup>13</sup>C COCAMQ spectrum and contributes a significant simplification of the spectra in the aliphatic region. This is a valid alternative to other available tools to quench such coupling.<sup>20,52</sup> Once the signals are detected, paramagnetic-based restraints<sup>7</sup> can be used for structural purposes.

In conclusion, the set of 2D NMR experiments (CT-COSY, COCAMQ, NOESY) based exclusively on <sup>13</sup>C detection and the implementation of band-selective homodecoupling to simplify multiplet structures in 2D spectra allow the detection of fast-relaxing signals in crowded regions of the spectra when the attached protons are broadened beyond detectable limits. Such experiments are feasible with the standard hardware optimized for <sup>1</sup>H detection conventionally used for triple resonance experiments. We have shown that going from <sup>1</sup>H to <sup>13</sup>C direct detection, with a conventional spectrometer set up, already allows us to significantly reduce the blind sphere around the paramagnetic center (for example, from 11 to 6 Å in case of type II Cu(II)). Of course, the use of probes optimized for <sup>13</sup>C sensitivity such as TXO and <sup>13</sup>C DUAL <sup>13</sup>C{<sup>1</sup>H} CryoProbe contributes to further reduction of the blind sphere so that it is

now limited to only the Cu(II) ligand imidazoles. Moreover, higher sensitivity implies a shorter experimental time for the same experiment; that is the key to permit higher dimensionality experiments. We believe that the technological advances necessary to fully exploit <sup>13</sup>C–<sup>13</sup>C{<sup>15</sup>N} NMR spectroscopy will represent a breakthrough for the application of NMR spectroscopy to paramagnetic proteins and, most importantly, to all the systems that suffer from fast transverse relaxation. They will therefore open new avenues for the application of NMR to systems with large molecular mass.

**Acknowledgment.** We thank Mr. Oskar Schett for the stimulating discussions and Dr. Paul Barker for the useful comments on the manuscript. This work was supported in part by the EC Contracts QLG2-CT-2002-00988 and HPRI-CT-2001-50026.

**Supporting Information Available:** Selected pulse sequences for <sup>13</sup>C–<sup>13</sup>C 2D experiments and experimental details (PDF). This material is available free of charge via the Internet at <http://pubs.acs.org>.

(52) Shimba, N.; Stern, A. S.; Craik, C. S.; Hoch, J. C.; Dötsch, V. *J. Am. Chem. Soc.* **2003**, *125*, 2382–2383.

JA037676P